Liquid-Liquid Transition in a Machine-Learned Coarse-grained Water Model

Debdas Dhabal[a], Rajat Kumar[a], and Valeria Molinero[a,*]

[a]Department of Chemistry, The University of Utah, Salt Lake City, UT 84112-0850, USA.

ABSTRACT. Mounting experimental evidence supports the existence of a liquid-liquid transition (LLT) in high-pressure supercooled water. However, fast crystallization of supercooled water impedes the identification of the LLT line $T_{LL}(p)$ in experiments. While the most accurate all-atom (AA) water models display a LLT, their computational cost limits investigations of its interplay with ice formation. Coarse-grained (CG) models provide over 100-fold computational efficiency gain over AA models, enabling the study of water crystallization, but have not yet shown to have a LLT. Here we demonstrate that the CG machine-learned water model ML-BOP has a LLT that ends in a critical point at p_c = 170±10 MPa and T_c = 181±3 K. The $T_{LL}(p)$ of ML-BOP is almost identical to the one of TIP4P/2005, adding to the similarity in the equation of state of liquid water in both models. The simulations reveal that $T_{LL}(p)$ coincides with the line of maximum crystallization rate $T_x(p)$ of supercooled ML-BOP, supporting a mechanistic relationship between the structural transformation in liquid water and the formation of ice.

The existence of a liquid-liquid phase transition (LLT) in supercooled water has been debated for over three decades.[1,2] The low-density amorphous (LDA) and high-density amorphous (HDA) ices are widely considered vitrified manifestations of the high and low density liquids (LDL and HDL), respectively, because of their sharp interconversion on compression and expansion has hysteresis typical of first order transitions.[3-5] However, it is not a foregone conclusion that the two non-equilibrium amorphous phases are the glasses of two distinct equilibrium liquids.[6]

Isobaric cooling experiments have not been able to provide direct evidence of a liquid-liquid transition because water crystallization takes place before a transformation between the metastable liquids can be detected.[7] However, recent ultrafast isochoric laser heating of HDA and LDA to drive water across the anticipated LLT have reported signatures consistent with the presence of such a liquid-liquid transformation just before supercooled water crystallizes to ice I.[8,9]

Despite decades of efforts, the liquid-liquid transition line $T_{LL}(p)$ has not yet been directly established in experiments. The experi[10]mental limits of stability of LDA and HDA upon isothermal decompression extrapolate to a possible liquid-liquid critical point (LLCP) with critical temperature $T_c \approx 180$ K and critical pressure $p_c \approx 200$ MPa.[11] However, equations of state (EOS) of water parameterized from stable and supercooled liquid water support a LLT that ends at a LLCP with p_c between 27 and 125 MPa.[12-17]

Several all-atom water models have a liquid-liquid transition. These include the rigid nonpolarizable ST2,[18,19] TIP4P/2005[20] and TIP4P/Ice[20] models, as well as the flexible models q-TIP4P/F,[21] E3B3,[22] WAIL,[23] and the DPMD-SCAN neural network derived from DFT.[24] However, the high computational cost of all-atom models has hindered their use in addressing the interplay between LLT and crystallization observed in experiments.[8,9]

Coarse-grained (CG) models based on short-ranged anisotropic interactions (SRAI) are over 100 times computationally more efficient than the least expensive all atom models with long-range electrostatics.[25,26] The monatomic water model mW,[25] based on the Stillinger-Weber potential,[27] is the most studied of that class of models. While mW crystallizes in accessible simulation times,[28-31] it does not have a LLT.[32,33] The more recently developed Machine-Learned Bond-Order Potential (ML-BOP)[26] is a CG SRAI water model based on the Tersoff potential[34] that crystallizes in accessible simulation times,[35] while reproducing the anomalies and equation of state of liquid water with the accuracy of TIP4P/2005 and the experimental melting line of ice I_h with the accuracy of TIP4P/Ice.[35] ML-BOP captures well the pressure dependence of the height g_2 of the second peak of the oxygen-oxygen radial distribution function of water,[35] as well as the pressure-induced amorphization of ice I_h and the structure and phase behavior of LDA and HDA and their interconversion on compression and expansion.[36] In what follows we show that ML-BOP has a liquid-liquid transition, with a critical point very close to those of TIP4P/2005 and TIP4P/Ice models.[20,37] We further demonstrate that the liquid-liquid transition coincides with the temperature of maximum crystallization rate, and discuss how the interplay between the LLT and glass transition impacts the density of hyperquenched glasses and the pressure at which they display a maximum in long-range density correlations.

ML-BOP has a liquid-liquid transition.

One of the characteristics of a liquid approaching a critical point is the increase of the correlation length of density fluctuations. These long-range density fluctuations can be trapped during vitrification and appear as static correlations in the glass.[38] Debenedetti and coworkers demonstrated that glasses made by isobaric cooling of TIP4P/2005 display a pronounced maximum in long-range density correlations near the pressure of the LLCP of that model, while these correlations are muted in the mW model and inexistent in a Lennard-Jones fluid.[38] We cooled a periodic simulation cell with 8000 ML-BOP molecules from the liquid to the glass at 10 K ns^{-1} at various pressures, and characterize the extent of long-range correlations by extrapolation of the structure factor $S(q)$ to zero wavevector[38] (Supp. Info. A)

Figure 1 shows that ML-BOP displays a pronounced increase of long-range structural correlations at both negative and positive pressures. The increase in correlations at negative pressures arises from the instability of the liquid against cavitation,[35] while the increase at positive pressures is associated a phase transformation in the supercooled liquid. The extrapolated long-range correlations of ML-BOP at positive pressures are most pronounced at 180 MPa and 177 K (Figures 1a and 1b), suggesting that to be close to the location of the LLCP.

To determine the location of the LLT and LLCP of the ML-BOP model, we perform isothermal-isobaric simulations with a cell containing 192 molecules, following ref [24]. The small cell enables the sampling of phase coexistence between LDL and HDL through system-wide oscillations of the density and structure of the liquid as a function of time (Figures S3-S6), while also delaying the formation of ice. The timescales of the oscillations between the two liquids in ML-BOP are shorter than in all-atom models of water,[20,24] consistent with the faster translational dynamics of the coarse-gained model.[26] We sample the density ρ and potential energy E of the 192 water molecule periodic cell over 15 independent trajectories at each T and p, collecting data until the onset of crystallization (Figures S7-S8), and compute the free energy from the corresponding histograms. Figure 2 shows that the free energy profiles as a function of liquid density at pressure above 170 MPa have two well-defined minima, corresponding to the HDL and LDL phases. We identify the liquid-liquid line $T_{LL}(p)$ as the T-p loci where the two liquid phases have the same free energies (Figures 3a-b).

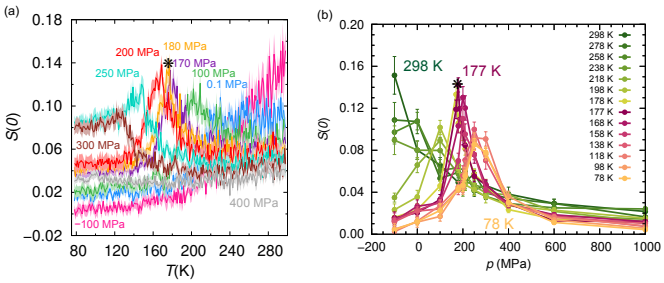

Figure 1. Long-range correlations in ML-BOP along vitrification simulations. The correlations are represented by the extrapolated zero wavenumber structure factor, S(0) as a function of (a) temperature and (b) pressure, computed from cooling simulations with 8000 water molecules at 10 K ns^{-1} rate following the procedure of ref. [38](see Figures S1 and S2 in Supp. Info. A). The uncertainties computed from 10 independent simulations are shown as shaded error regions in (a) and as error bars in (b). The amount of ice in the hyperquenched glasses at 77 K is ~5%,[39] consistent with the fraction of ice in experiments at the minimum cooling rate needed for vitrification of water.[40]

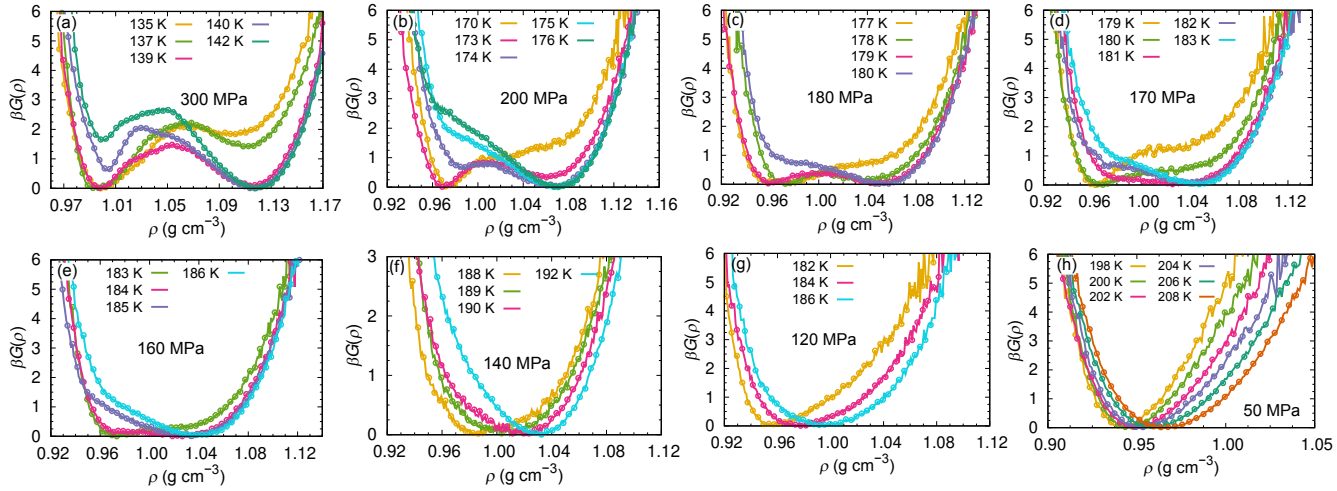

Figure 2. Free energy profiles of supercooled liquid ML-BOP as a function of density ρ, normalized by the thermal energy $\beta^{-1} = RT$. Each panel presents free energy profiles at the temperature indicated in the graphs and pressures (a) 300 MPa, (b) 200 MPa, (c) 180 MPa, (d) 170 MPa, (e) 160 MPa, (f) 140 MPa, (g) 120 MPa, (h) 50 MPa. We identify 170 MPa as the critical pressure: at p > 170 MPa there are temperatures with two basins for stable and/or metastable HDL and LDL, while at p < 170 MPa, there is only one minimum in the free energy landscape of the liquid.

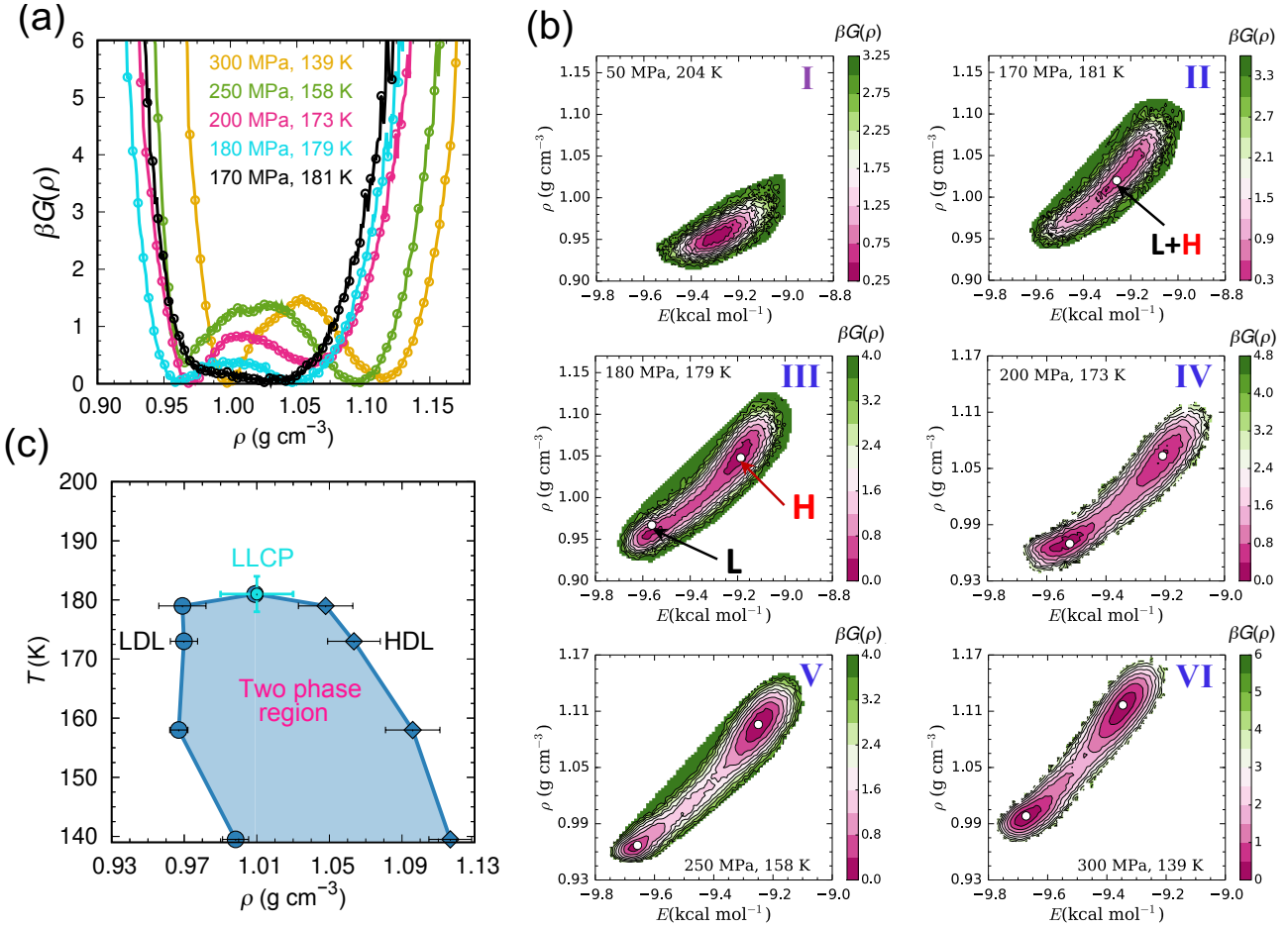

Figure 3. Liquid-liquid equilibrium in ML-BOP water. (a) Free energy as a function of density ρ along the LLT line. (b) Two-dimensional free energy as a function of density ρ and potential energy E for the state points of panel (a), as well as a supercritical liquid at 50 MPa and 204 K. The p and T are indicated in each I to VI panel. Panel (b)II corresponds to the LLCP. (c) T-ρ phase diagram of supercooled ML-BOP showing in light blue the region of two-phase coexistence.

The free energy basins for the two liquids merge at 170 MPa and 181 K (Figure 3a-b). As the maximum in extrapolated $S(0)$ at 170 MPa and 180 MPa are identical within their error bars (Figure 1a), we assess that the LLCP of ML-BOP is located at p_c = 170±10 MPa and T_c = 181±3 K. The critical density is ρ_c = 1.01±0.02, same as for TIP4P/2005 and TIP4P/Ice.[20] The LDL edge of the binodal of the LLT in ML-BOP has a negative dρ/dT slope (Figure 3c), consistent with predictions by EOS based on experimental water data.[8]

Figure 4 shows the liquid-liquid transition line $T_{LL}(p)$ in the phase diagram of ML-BOP. The LLCP of ML-BOP aligns closely with that reported for TIP4P/2005, TIP4P/Ice and other all-atom water models[17,18,20,22,23,41] (Table 1). Indeed, Figure S9 shows that the $T_{LL}(p)$ of ML-BOP is almost indistinguishable from the one predicted for TIP4P/2005 from its two-state equation of state (TSEOS).[37]

Table 1. Liquid-liquid critical pressure p_c and temperature T_c for various water models.

Water Model	p_c (MPa)	T_c (K)
ML-BOP	170±10	181±3
TIP4P/2005[(a)]	170	182
TIP4P/2005[(b)]	186.1±0.9	172±1
TIP4P/Ice[(c)]	173.9±0.6	188.6±1
TIP4P/Ice[(d)]	165±15	195±5
ST2[(e)]	167±24	237±4
E3B3[(f)]	210±10	180±2
WAIL[(g)]	36.5±0.8	210.5±0.3
DeePMD[(h)]	268.7±0.68	224±3
q-TIP4P/F[(i)]	167±9	159±6

(a) computed from TSEOS in ref. [37]; (b) computed from free energy calculations in ref. [20]; (c) computed from free energy calculations in ref. [20];(d) computed from Maxwell construction in ref. [17]; (e) computed using histogram reweighting monte carlo simulations in grand canonical ensemble in ref. [18]; (f) computed from the extrapolation of two widom

lines from k_T and C_p in ref. [22]; (g) computed from TSEOS in ref. [23]; (h) computed from TSEOS in ref. [41]; (i) computed from TSEOS in ref. [21].

It is intriguing that the LLCP of ML-BOP, TIP4P/2005, and TIP4P/Ice are in good agreement with the extrapolation of the crossing of the limit of stability of the low- and high-density amorphous ices in experiments,[8,11] although those extrapolations carry significant uncertainty. More recent analyses suggests that the experimental LLCP may be located around 195 to 210 K and 100 to 125 MPa.[10,13,17]

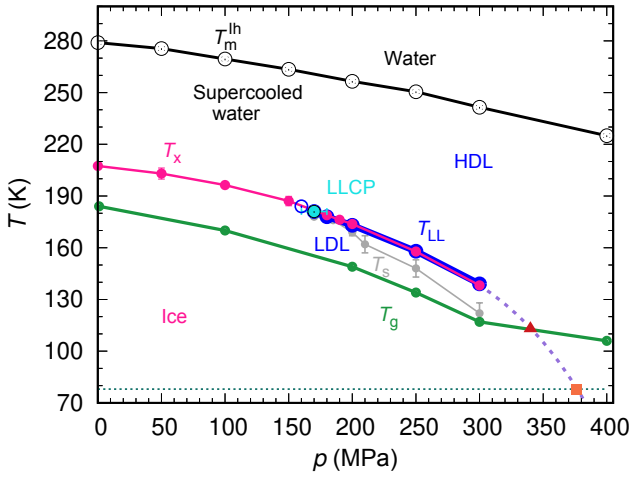

Figure 4. Phase diagram of ML-BOP water. The blue line shows the liquid-liquid transition line $T_{LL}(p)$ computed from free energy calculations. The cyan circle indicates the LLCP, located at p_c =170±10 MPa and T_c =181±3 K. The open blue circle is on the supercritical extension of the LLT. The black line shows the equilibrium melting line of hexagonal ice $T_m^{Ih}(p)$.[35] The magenta line shows the nonequilibrium line of maximum crystallization rate $T_x(p)$ determined by isobaric cooling of simulation cells with 8000 ML-BOP water molecules at the fastest cooling rate that crystallizes ML-BOP, 0.2 K ns^{-1}.[35] The green line represents the glass transition temperature $T_g(p)$ computed using mobility criteria over 10 K ns^{-1} cooling simulations (See Methods). The purple dashed line is the extrapolation of $T_x(p)$ using a 3rd order polynomial, which we assume to extrapolate $T_{LL}(p)$. The gray line shows the temperature of maximum structural correlations $T_S(p)$ upon isobaric cooling at 10 K ns^{-1}. The red triangle at 340 MPa and 130 K indicates the intersection of the extrapolated $T_{LL}(p)$ with $T_g(p)$. The orange square at 376 MPa represents the extrapolated $T_{LL}(p)$ to 78 K.

Ice crystallization is fastest at the LLT.

The identification of the locus of the LLT in experiments has been hindered by fast ice crystallization. The minimum cooling rate required to avoid crystallization of water droplets is 10^{-2} to10^{-3} K ns^{-1} [40] in experiments and 1 K ns^{-1} in simulations with ML-BOP.[35] This suggests that the dynamics of deeply supercooled ML-BOP is ~100 to 1000 times faster than in water. Considering the 100 fold increase in computational efficiency of the CG model,[26] the sampling of the free energy landscape in simulations with ML-BOP is 10^4 to 10^5-fold more efficient than with all-atom models that accurately reproduce the dynamics of water, such as TIP4P/2005.[42,43] These combined efficiencies enable studies of crystallization with ML-BOP without the need of enhanced sampling methods.[35,39]

The line of temperatures $T_x(p)$ at which ice crystallization is the fastest demarcates the boundary between nucleation-limited and growth-limited regimes (above and below $T_x(p)$, respectively).[30] Previous analysis using classical nucleation theory with experimental data for water and molecular simulations with the mW model predicted that the temperature T_x at which the crystallization rate of water is maximum coincides with the Widom line.[30] These predictions were later confirmed by experiments at ambient pressure that locate T_x at 228±1 K,[44] indistinguishable from the 229±1 K of the maxima in C_p[45] and K_T.[46] Figure 4 reveals that the coincidence between the temperature of maximum crystallization rate $T_x(p)$ and the locus of structural transformation of supercooled water extends to the first-order LLT line, suggesting that the formation of the low-density liquid, or pronounced LDL-like fluctuations in the high-density liquid in the proximity of its spinodal, result in a combination of low ice nucleation barriers with significant mobility that enables fast growth of ice.

The alignment between $T_{LL}(p)$ and $T_x(p)$ suggests a close relationship between the liquid-liquid transition of water and the homogeneous nucleation line $T_{hom}(p)$ established by Angell and coworkers.[47] At 0.1 MPa T_{hom} of ref. [47] stands 7 K above both the maximum crystallization[44] and Widom[45,46] temperatures of water. A recent estimation of water's LLCP, derived from calculations involving TIP4P/Ice and comparison with experimental liquid EOS, suggests the LLCP to be twice farther from T_{hom}, at 195 K and 125 MPa.[17] We note, however that crystallization data alone is insufficient to locate the pressure of the LLCP: the experimental $T_{hom}(p)$[47] does not show any anomaly within the pressure range where the LLCP of water is anticipated, nor does $T_x(p)$ in our simulations.

Vitrification arrests the LLT far from the critical point.

The experimental glass transition of water is below the proposed liquid-liquid transition line.[5] That is also the case for ML-BOP, which has $T_g(p) < T_{LL}(p)$ for $p < 350$ MPa (Figure 4). $T_g(p)$ shown in Figure 4 corresponds to the locus where the molecules displace less than 0.8 Å over 100 ps in 10 K ns^{-1} cooling simulations. This definition results in $T_g(p)$ higher than in experiments,[48] yet the model correctly produces the negative slope of the glass transition line with pressure reported for all-atom models of water[40] and experiments.[5,49]

In principle, the HDL to LDL transition can be completed prior to vitrification in cooling simulations at pressures between p_c = 170±10 MPa and ~340 MPa, for which $T_g(p) < T_{LL}(p)$. However, at the high cooling rates required to bypass crystallization the liquid-liquid transformation occurs below the equilibrium $T_{LL}(p)$. The locus of the non-equilibrium transformation can be gleaned from the temperatures $T_S(p)$ of maximum $S(0)$ along the cooling simulations (Figure 1).

$T_S(p)$ is an effective limit of stability of HDL, although it needs not coincide with the thermodynamic spinodal.

$T_S(p)$ of ML-BOP starts at the LLCP and crosses the glass transition line at 300 MPa (Figure 4). Vitrification truncates the HDL to LDL transformation at 250 to 300 MPa (Figure 1), freezing in the largest long-range correlations at pressures well above p_c = 170±10 MPa of the model. As water also has $T_g(p) < T_{LL}(p)$, we anticipate that the highest $S(0)$ will be found in glasses prepared at pressures well above p_c.

Glasses that vitrify as they undergo the LLT have densities comparable of medium density amorphous ice.

The density of the glasses obtained by isobaric hyperquenching of ML-BOP display a sigmoidal shape with maximum slope between 250 and 300 MPa (Figure 5).[39] These are the pressures at which ML-BOP glasses present the largest long-range density correlations (Figure 1), because they vitrify as they transition from HDL to LDL.

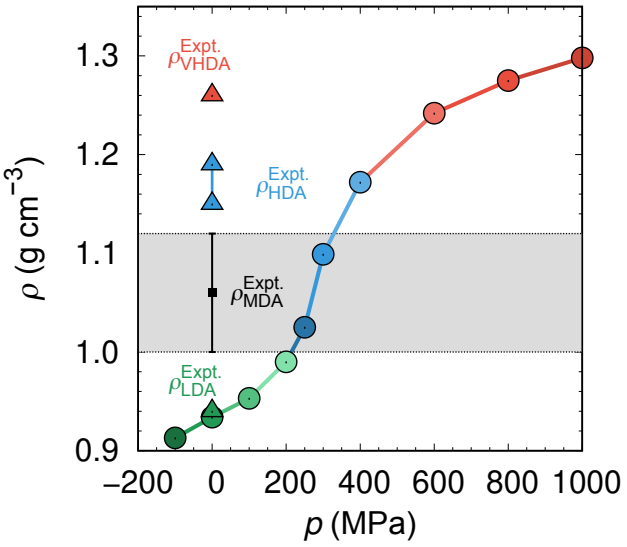

Figure 5. Densities of hyperquenched glasses produced by isobaric cooling of ML-BOP at 10 K ns^{-1} to 78 K (Adapted from ref [39]). Circles show the density of the ML-BOP glasses; triangles show the experimental densities at 0.1 MPa of LDA (green),[50,51] HDA (blue),[52-56] VHDA (red),[56] and MDA(black).[57] The density of the HQG prepared at 250 and 300 MPa falls with the the 1.06 ± 0.06 g cm^{-3} density range of MDA (gray band) prepared at unknown pressure and shear rates before recovering it at 0.1 MPa.[57]

Hyperquenched glasses obtained at 250 to 300 MPa are in the density range of the recently uncovered medium density amorphous ice (MDA) made by ball-milling ice at 77 K and recovered at 0.1 MPa[57] (Figure 5). However, the HQG with density intermediate between those of LDA and HDA have significant long-range structural correlations (Figure 1), while there are no strong signatures in the low q region of $S(q)$ of MDA (if there are, they are hidden under strong Porod-law dispersion).[57] It is not yet known whether the shearing involved in ball-milling enables the sampling of distinct states not visited during hyperquenching protocols, or there are equivalencies in the structure and thermodynamics of ball-milled and hyperquenched water glasses.

Conclusions and outlook.

The existence of a liquid-liquid transition has been the focus of the debate over the origin of water anomalies since it was proposed from pioneering molecular simulations with the ST2 model.[1] Intense research in the last years has established that the most accurate all-atom models of water have a liquid-liquid transition.[18,20-23] However, a LLT had not been found in coarse-grained water models. In the present study, we demonstrate that the monatomic machine-learned model ML-BOP has a liquid-liquid transition that ends in a critical point at p_c = 170±10 MPa and T_c = 181±3K. Significantly, the liquid-liquid transition line and critical point of ML-BOP closely align with predictions made for the all-atom TIP4P/2005 water model,[20,37] bolstering the likeness of the equations of state (EOS) of these models.[35,39]

The expense of all-atom models has limited the modeling of the competition between LLT and crystallization observed in experiments.[8,9] The coarse-grained nature of ML-BOP endows it with 10^4 to 10^5 increase in efficiency of the sampling of the free energy landscape compared to all-atom water models, uniquely positioning ML-BOP for the investigation of the interplay between liquid-liquid transition and crystallization in deeply supercooled water.

Our simulations with ML-BOP reveal that the coincidence of the temperature of maximum crystallization rate T_x and maximum change in the structure and thermodynamics of supercooled liquid water[30] carry forward to the first-order liquid-liquid line. Nevertheless, accurately identifying the locus of the liquid-liquid transition of water, particularly its critical pressure, remains a formidable challenge. This challenge persists because the LLCP does not manifest a discernible signature during ice crystallization. Additionally, our findings indicate that under rapid cooling rates sufficient to prevent crystallization, the peak in long-range correlations in hyperquenched glasses emerges well beyond the critical pressure, at the intersection of the glass transition line and the nonequilibrium liquid-liquid transformation during cooling. New approaches are needed to determine the LLT and LLCP in experiments. The accessibility to the liquid-liquid transition and competing ice crystallization in ML-BOP makes it a promising tool to complement these measurements and guide their interpretation.

METHODS

Molecular dynamics simulations are performed with the ML-BOP water model[26] using LAMMPS[58] in the NpT ensemble with a time step of 5 fs using periodic cubic simulation cells with periodic boundary conditions in the three Cartesian directions. The temperature and pressure are controlled with the Nose-Hoover thermostat and barostat with time

constants of 0.5 and 5 ps, respectively. The initial configurations for all liquid simulation boxes are generated using Packmol.[59]

We calculate the zero wave number structure factor S(0) of liquid and vitrified ML-BOP along isobaric cooling simulations at 10 K ns^{-1} from 298 K to 78 K at p= -100, 0.1, 100, 170, 180, 200, 250, 300, 400, 600, and 1000 MPa following the procedure of ref. [38] (see Supp. Info. A). S(0) at each T and p is averaged over 10 independent cooling simulations. We report the standard deviation among these 10 simulations as the error bar. We use the CHILL+ algorithm[60] to compute the amount of ice in the glasses.

To determine the liquid-liquid transition line $T_{LL}(p)$ we perform NpT simulations with cells containing 192 ML-BOP molecules at the T and p listed Table 2. We evolve 15 independent 500 ns long simulations at each thermodynamic condition (T, p), each initialized with different sets of random velocities consistent with the selected temperature. The small size of the cell enables heterophasic oscillations as a function of time[61] between high- and low-density liquid, before crystallization takes over. Figure S5 shows that fluctuation in density between LDL and HDL correlates with the fraction of 4-coordinated water molecules in the liquid. We collect density ρ and potential energy E of the system until 12 water molecules (6% of the total) are classified as ice I using CHILL+. Smaller ice crystallites are subcritical and do not lead to ice formation in the whole cell.

Table 2: The range of temperatures at which we perform simulations to calculate the free energy diagrams.

P(MPa)	Temperatures (K)
300	135, 136, 136.5, 137, 137.5, 139, 140, 142
250	156, 157, 158, 159, 160
200	170, 173, 174, 175, 176, 178, 183
180	177, 178, 179, 180, 184
170	179, 180, 181, 182,183
160	183, 184, 185, 186, 188,190
50	198, 200, 202,203, 204, 206, 207, 208, 212

We build probability histograms of observing a particular density and energy $P(E, \rho)$ from this collection of trajectories, from which we compute the free energies: $\beta G(E, \rho) = -\ln[P(E, \rho)]$, where $\beta = (K_b T)^{-1}$. We calculate one-dimensional probability and corresponding free energy profiles as a function of density by integrating out energy (E) from the two-dimensional free energy surfaces, $\beta G(E, \rho)$. The regions with two minima in the free energy are further analyzed to identify the T and p of equilibrium between the two liquids as the loci for which the basins of LDL and HDL have approximately the same populations.

The temperature of maximum crystallization rate $T_x(p)$ at p = 0, 50, 100, 150, 200, 250 and 300 MPa was determined in ref. [35] as an average of the onset temperature of crystallization over 5 independent cooling simulations at 0.2 Kns^{-1} for each pressure. Here we follow the same procedure to compute $T_x(p)$ at 170, 180 and 190 MPa.

We calculate the glass transition temperature as a function of pressure $T_g(p)$ considering the mobility criteria. The temperature at which the mean displacement of the particles becomes less than 0.8 Å at a certain pressure in the cooling simulations with a 10 K ns^{-1} rate is estimated to be the glass transition temperature (T_g). The mean displacement of the particle becomes insensitive to further lowering in temperature below the estimated T_g. Furthermore, we visualize the cooling trajectory to ensure the dynamic freezing of the water molecules.

ACKNOWLEDGMENTS

This work was supported by the U.S. Air Force Office of Scientific Research through MURI Award FA9550-20-1-0351. We thank Ingrid de Almeida Ribeiro for discussions and the Center of High-Performance Computing at The University of Utah for technical support and an award of computing time.

ASSOCIATED CONTENT

Supporting Information

The Supporting Information includes in Section A a comparison of $S(0)$ estimated using different fitting functions for $S(q)$ and the isothermal compressibility of ML-BOP; in section B the density and fractions of high and low coordinated liquids and ice for the 192 molecule cell as a function of time, as well as snapshots of the simulation cell showing the formation of liquid-liquid interface near the barrier region at 300 MPa and 139 K; section C contains a T-p phase diagram showing the melting line of ML-BOP, TIP4P/2005, TIP4P/Ice and water in experiments, as well as the liquid-liquid line for ML-BOP and for TIP4P/2005 according to a two-state equation of state.

AUTHOR INFORMATION

Corresponding Author

Valeria Molinero – Department of Chemistry, The University of Utah, Salt Lake City, Utah 84112-0850, United States.

orcid.org/0000-0002-8577-4675;

Email: valeria.molinero@utah.edu

Authors

Debdas Dhabal – Department of Chemistry, The University of Utah, Salt Lake City, Utah 84112-0850, United States.

orcid.org/0000-0003-1534-1599;

Rajat Kumar – Department of Chemistry, The University of Utah, Salt Lake City, Utah 84112-0850, United States.

REFERENCES

1 Poole, P. H., Sciortino, F., Essmann, U. & Stanley, H. E. Phase behaviour of metastable water. *Nature* **360**, 324-328 (1992). https://doi.org:10.1038/360324a0

2 Palmer, J. C., Poole, P. H., Sciortino, F. & Debenedetti, P. G. Advances in Computational Studies of the Liquid–Liquid Transition in

Water and Water-Like Models. *Chem. Rev.* **118**, 9129-9151 (2018). https://doi.org:10.1021/acs.chemrev.8b00228
3 Mishima, O. & Stanley, H. E. The relationship between liquid, supercooled and glassy water. *Nature* **396**, 329-335 (1998). https://doi.org:10.1038/24540
4 Debenedetti, P. G. & Stillinger, F. H. Supercooled liquids and the glass transition. *Nature* **410**, 259-267 (2001). https://doi.org:10.1038/35065704
5 Gallo, P. *et al.* Water: A Tale of Two Liquids. *Chem. Rev.* **116**, 7463-7500 (2016). https://doi.org:10.1021/acs.chemrev.5b00750
6 Limmer, D. T. & Chandler, D. Theory of amorphous ices. *Proc. Natl. Acad. Sci.* **111**, 9413-9418 (2014). https://doi.org:10.1073/pnas.1407277111
7 Debenedetti, P. G. & Stanley, H. E. Supercooled and Glassy Water. *Phys. Today* **56**, 40-46 (2003). https://doi.org:10.1063/1.1595053
8 Amann-Winkel, K. *et al.* Liquid-liquid phase separation in supercooled water from ultrafast heating of low-density amorphous ice. *Nat. Commun.* **14**, 442 (2023). https://doi.org:10.1038/s41467-023-36091-1
9 Kim, K. H. *et al.* Experimental observation of the liquid-liquid transition in bulk supercooled water under pressure. *Science* **370**, 978-982 (2020). https://doi.org:10.1126/science.abb9385
10 Hestand, N. J. & Skinner, J. Perspective: Crossing the Widom line in no man's land: Experiments, simulations, and the location of the liquid-liquid critical point in supercooled water. *J. Chem. Phys.* **149** (2018).
11 Bachler, J., Giebelmann, J. & Loerting, T. Experimental evidence for glass polymorphism in vitrified water droplets. *Proc. Natl. Acad. Sci.* **118**, e2108194118 (2021). https://doi.org:10.1073/pnas.2108194118
12 Holten, V., Bertrand, C. E., Anisimov, M. A. & Sengers, J. V. Thermodynamics of supercooled water. *The Journal of Chemical Physics* **136**, 094507 (2012). https://doi.org:10.1063/1.3690497
13 Mishima, O. & Sumita, T. Equation of State of Liquid Water Written by Simple Experimental Polynomials and the Liquid–Liquid Critical Point. *J Phys Chem B* **127**, 1414-1421 (2023).
14 Mishima, O. Volume of supercooled water under pressure and the liquid-liquid critical point. *The Journal of Chemical Physics* **133**, 144503 (2010). https://doi.org:10.1063/1.3487999
15 Holten, V., Sengers, J. V. & Anisimov, M. A. Equation of State for Supercooled Water at Pressures up to 400 MPa. *Journal of Physical and Chemical Reference Data* **43**, 043101 (2014). https://doi.org:10.1063/1.4895593
16 Moynihan, C. T. Two Species/Nonideal Solution Model for Amorphous/Amorphous Phase Transitions. *MRS Online Proceedings Library* **455**, 411-425 (1996). https://doi.org:10.1557/PROC-455-411
17 Espinosa, J. R., Abascal, J. L. F., Sedano, L. F., Sanz, E. & Vega, C. On the possible locus of the liquid–liquid critical point in real water from studies of supercooled water using the TIP4P/Ice model. *J. Chem. Phys.* **158** (2023).
18 Liu, Y., Panagiotopoulos, A. Z. & Debenedetti, P. G. Low-temperature fluid-phase behavior of ST2 water. *J. Chem. Phys.* **131**, 104508 (2009). https://doi.org:10.1063/1.3229892
19 Palmer, J. C., Martelli, F., Liu, Y., Car, R., Panagiotopoulos, A. Z. & Debenedetti, P. G. Metastable liquid–liquid transition in a molecular model of water. *Nature* **510**, 385-388 (2014). https://doi.org:10.1038/nature13405
20 Debenedetti, P. G., Sciortino, F. & Zerze, G. H. Second critical point in two realistic models of water. *Science* **369**, 289-292 (2020). https://doi.org:10.1126/science.abb9796
21 Eltareb, A., Lopez, G. E. & Giovambattista, N. Evidence of a liquid–liquid phase transition in H2O and D2O from path-integral molecular dynamics simulations. *Sci. Rep.* **12**, 6004 (2022). https://doi.org:10.1038/s41598-022-09525-x
22 Ni, Y. & Skinner, J. L. Evidence for a liquid-liquid critical point in supercooled water within the E3B3 model and a possible interpretation of the kink in the homogeneous nucleation line. *J. Chem. Phys.* **144**, 214501 (2016). https://doi.org:10.1063/1.4952991
23 Weis, J., Sciortino, F., Panagiotopoulos, A. Z. & Debenedetti, P. G. Liquid–liquid criticality in the WAIL water model. *J. Chem. Phys.* **157**, 024502 (2022). https://doi.org:10.1063/5.0099520
24 Gartner, T. E., Piaggi, P. M., Car, R., Panagiotopoulos, A. Z. & Debenedetti, P. G. Liquid-Liquid Transition in Water from First Principles. *Phys. Rev. Lett.* **129**, 255702 (2022). https://doi.org:10.1103/physrevlett.129.255702
25 Molinero, V. & Moore, E. B. Water Modeled As an Intermediate Element between Carbon and Silicon. *J Phys Chem B* **113**, 4008-4016 (2009). https://doi.org:10.1021/jp805227c
26 Chan, H. *et al.* Machine learning coarse grained models for water. *Nat. Commun.* **10**, 379 (2019). https://doi.org:10.1038/s41467-018-08222-6
27 Stillinger, F. H. & Weber, T. A. Computer simulation of local order in condensed phases of silicon. *Phys. Rev. B* **31**, 5262-5271 (1984). https://doi.org:10.1103/physrevb.31.5262
28 Johnston, J. C. & Molinero, V. Crystallization, Melting, and Structure of Water Nanoparticles at Atmospherically Relevant Temperatures. *J Am Chem Soc* **134**, 6650-6659 (2012). https://doi.org:10.1021/ja210878c
29 Moore, E. B. & Molinero, V. Ice crystallization in water's "no-man's land". *J. Chem. Phys.* **132**, 244504 (2010). https://doi.org:10.1063/1.3451112
30 Moore, E. B. & Molinero, V. Structural transformation in supercooled water controls the crystallization rate of ice. *Nature* **479**, 506-508 (2011). https://doi.org:10.1038/nature10586
31 Moore, E. B. & Molinero, V. Is it cubic? Ice crystallization from deeply supercooled water. *Phys. Chem. Chem. Phys.* **13**, 20008-20016 (2011). https://doi.org:10.1039/c1cp22022e
32 Holten, V., Limmer, D. T., Molinero, V. & Anisimov, M. A. Nature of the anomalies in the supercooled liquid state of the mW model of water. *J. Chem. Phys.* **138**, 174501 (2013). https://doi.org:10.1063/1.4802992
33 Limmer, D. T. & Chandler, D. The putative liquid-liquid transition is a liquid-solid transition in atomistic models of water. *J. Chem. Phys.* **135**, 134503 (2011). https://doi.org:10.1063/1.3643333
34 Tersoff, J. New empirical model for the structural properties of silicon. *Phys. Rev. Lett.* **56**, 632-635 (1986). https://doi.org:10.1103/physrevlett.56.632
35 Dhabal, D., Sankaranarayanan, S. K. R. S. & Molinero, V. Stability and Metastability of Liquid Water in a Machine-Learned Coarse-Grained Model with Short-Range Interactions. *J Phys Chem B* **126**, 9881-9892 (2022). https://doi.org:10.1021/acs.jpcb.2c06246
36 Dhabal, D. & Molinero, V. Kinetics and Mechanisms of Pressure-Induced Ice Amorphization and Polyamorphic Transitions in a Machine-Learned Coarse-Grained Water Model. *The Journal of Physical Chemistry B* **127**, 2847-2862 (2023).
37 Singh, R. S., Biddle, J. W., Debenedetti, P. G. & Anisimov, M. A. Two-state thermodynamics and the possibility of a liquid-liquid phase transition in supercooled TIP4P/2005 water. *J. Chem. Phys.* **144**, 144504 (2016). https://doi.org:10.1063/1.4944986
38 Gartner, T. E., Torquato, S., Car, R. & Debenedetti, P. G. Manifestations of metastable criticality in the long-range structure of model water glasses. *Nat. Commun.* **12**, 3398 (2021). https://doi.org:10.1038/s41467-021-23639-2

39 Dhabal, D. & Molinero, V. Kinetics and Mechanisms of Pressure-induced Ice Amorphization and Polyamorphic Transitions in a Machine-learned Coarse-Grained Water Model. (2023). https://doi.org:10.26434/chemrxiv-2023-llft6
40 Kohl, I., Mayer, E. & Hallbrucker, A. The glassy water–cubic ice system: a comparative study by X-ray diffraction and differential scanning calorimetry. *Phys. Chem. Chem. Phys.* **2**, 1579-1586 (2000). https://doi.org:10.1039/a908688i
41 Gartner, T. E., Zhang, L., Piaggi, P. M., Car, R., Panagiotopoulos, A. Z. & Debenedetti, P. G. Signatures of a liquid–liquid transition in an ab initio deep neural network model for water. *Proc. Natl. Acad. Sci.* **117**, 26040-26046 (2020). https://doi.org:10.1073/pnas.2015440117
42 Rozmanov, D. & Kusalik, P. G. Transport coefficients of the TIP4P-2005 water model. *J. Chem. Phys.* **136**, 044507 (2012). https://doi.org:10.1063/1.3677196
43 Abascal, J. L. F. & Vega, C. A general purpose model for the condensed phases of water: TIP4P/2005. *J. Chem. Phys.* **123**, 234505 (2005). https://doi.org:10.1063/1.2121687
44 Laksmono, H. *et al.* Anomalous Behavior of the Homogeneous Ice Nucleation Rate in "No-Man's Land". *J. Phys. Chem. Lett.* **6**, 2826-2832 (2015). https://doi.org:10.1021/acs.jpclett.5b01164
45 Pathak, H. *et al.* Enhancement and maximum in the isobaric specific-heat capacity measurements of deeply supercooled water using ultrafast calorimetry. *Proc. Natl. Acad. Sci.* **118**, e2018379118 (2021). https://doi.org:10.1073/pnas.2018379118
46 Kim, K. H. *et al.* Maxima in the thermodynamic response and correlation functions of deeply supercooled water. *Science* **358**, 1589-1593 (2017). https://doi.org:10.1126/science.aap8269
47 Kanno, H., Speedy, R. & Angell, C. Supercooling of water to-92 C under pressure. *Science* **189**, 880-881 (1975).
48 Angell, C. A. Insights into Phases of Liquid Water from Study of Its Unusual Glass-Forming Properties. *Science* **319**, 582-587 (2008). https://doi.org:10.1126/science.1131939
49 Giovambattista, N., Loerting, T., Lukanov, B. R. & Starr, F. W. Interplay of the Glass Transition and the Liquid-Liquid Phase Transition in Water. *Sci. Rep.* **2**, 390 (2012). https://doi.org:10.1038/srep00390
50 Loerting, T., Salzmann, C., Kohl, I., Mayer, E. & Hallbrucker, A. A second distinct structural " state " of high-density amorphous ice at 77 K and 1 bar. *Phys. Chem. Chem. Phys.* **3**, 5355-5357 (2001). https://doi.org:10.1039/b108676f
51 Winkel, K., Bowron, D. T., Loerting, T., Mayer, E. & Finney, J. L. Relaxation effects in low density amorphous ice: Two distinct structural states observed by neutron diffraction. *J. Chem. Phys.* **130**, 204502 (2009). https://doi.org:10.1063/1.3139007
52 Mariedahl, D. *et al.* X-ray Scattering and O–O Pair-Distribution Functions of Amorphous Ices. *J Phys Chem B* **122**, 7616-7624 (2018). https://doi.org:10.1021/acs.jpcb.8b04823
53 Amann-Winkel, K., Bowron, D. T. & Loerting, T. Structural differences between unannealed and expanded high-density amorphous ice based on isotope substitution neutron diffraction. *Mol. Phys.* **117**, 3207-3216 (2019). https://doi.org:10.1080/00268976.2019.1649487
54 Mishima, O., Calvert, L. D. & Whalley, E. 'Melting ice' I at 77 K and 10 kbar: a new method of making amorphous solids. *Nature* **310**, 393-395 (1984). https://doi.org:10.1038/310393a0
55 Mishima, O., Calvert, L. D. & Whalley, E. An apparently first-order transition between two amorphous phases of ice induced by pressure. *Nature* **314**, 76-78 (1985). https://doi.org:10.1038/314076a0
56 Loerting, T., Salzmann, C. G., Winkel, K. & Mayer, E. The relation between high-density and very-high-density amorphous ice. *Phys. Chem. Chem. Phys.* **8**, 2810-2818 (2006). https://doi.org:10.1039/b603159e
57 Rosu-Finsen, A. *et al.* Medium-density amorphous ice. *Science* **379**, 474-478 (2023). https://doi.org:10.1126/science.abq2105
58 Plimpton, S. Fast Parallel Algorithms for Short-Range Molecular Dynamics. *Journal of Computational Physics* **117**, 1-19 (1995). https://doi.org:https://doi.org/10.1006/jcph.1995.1039
59 Martínez, J. M. & Martínez, L. Packing optimization for automated generation of complex system's initial configurations for molecular dynamics and docking. *Journal of Computational Chemistry* **24**, 819-825 (2003). https://doi.org:https://doi.org/10.1002/jcc.10216
60 Nguyen, A. H. & Molinero, V. Identification of Clathrate Hydrates, Hexagonal Ice, Cubic Ice, and Liquid Water in Simulations: the CHILL+ Algorithm. *The Journal of Physical Chemistry B* **119**, 9369-9376 (2015). https://doi.org:10.1021/jp510289t
61 Kastelowitz, N. & Molinero, V. Ice–Liquid Oscillations in Nanoconfined Water. *ACS Nano* **12**, 8234-8239 (2018). https://doi.org:10.1021/acsnano.8b03403